ELSEVIER

International Journal of Heat and Fluid Flow 20 (1999) 196–207

International Journal of HEAT AND FLUID FLOW

www.elsevier.com/locate/ijhff

DNS of turbulent heat transfer in channel flow with respect to Reynolds and Prandtl number effects

Hiroshi Kawamura [a,*], Hiroyuki Abe [a], Yuichi Matsuo [b]

[a] *Department of Mechanical Engineering, Science University of Tokyo, Noda-shi, Chiba-ken 278-8510, Japan*
[b] *National Aerospace Laboratory, Chofu-shi, Tokyo 182-8522, Japan*

Abstract

The direct numerical simulation (DNS) of turbulent heat transfer in a channel flow has been carried out to investigate the Reynolds and Prandtl number effects on the turbulent heat transport. The configuration is a fully developed turbulent channel flow with uniform heating from both walls. The Reynolds numbers based on the friction velocity and the channel half width are 180 and 395, and the molecular Prandtl numbers are 0.025, 0.2 and 0.71. The statistical quantities such as the temperature variance, turbulent heat fluxes, turbulent Prandtl number and the time scale ratio are obtained and the effects of the Reynolds and Prandtl numbers are examined. Budget terms of the temperature variance and the turbulent heat fluxes are also calculated. In addition, the instantaneous flow and thermal fields are visualized in order to investigate the structures of streaks and vortices.

Keywords: DNS; Turbulent heat transfer; Channel flow; Turbulent Prandtl number; Time scale ratio

Notation

a_t	thermal eddy-diffusivity
b_i, c_i, d_i	coefficient of expansion
c_p	specific heat at constant pressure
k	turbulent kinetic energy
p	pressure
Pe_τ	Peclet number $= \mathrm{Pr} \cdot \mathrm{Re}_\tau$
Pr	molecular Prandtl number
Pr_t	turbulent Prandtl number
P_θ	production term of temperature variance
q_w	wall heat flux
q_{total}	total heat flux
R	time constant ratio
$R_{\phi\psi}$	cross-correlation coefficient $= \overline{\phi\psi}/\phi_{rms}\psi_{rms}$
Re_τ	Reynolds number $= u_\tau \delta/\nu$
Re_m	Reynolds number $= \langle \overline{u}^+ \rangle\, 2\delta/\nu$
t	time
T	temperature
T_m	bulk mean temperature
T_τ	friction temperature $= q_w/\rho c_p u_\tau$
u_i, u, v, w	velocity component
u_τ	friction velocity $= \sqrt{\tau_w/\rho}$
x_1, x	streamwise direction
x_2, y	wall-normal direction
x_3, z	spanwise direction

Greek

δ	channel half width
ε	dissipation of turbulent energy
ε_θ	dissipation of temperature variance
κ_θ	Karman constant of mean temperature
θ	transformed temperature
ν	kinematic viscosity
ν_t	eddy-diffusivity
ρ	density
τ_w	statistically averaged wall shear stress

Superscripts

$(\,)^*$	normalized by δ
$(\,)^+$	normalized by u_τ, ν and T_τ
$(\,)'$	fluctuation component
$\overline{(\,)}$	statistically averaged
$\langle\,\rangle$	averaged over channel section
$(\,)_{rms}$	root mean square

1. Introduction

The direct numerical simulations (DNSs) of turbulent heat transfer are now widely performed for various configurations. Among them, the DNS of the fully developed turbulent channel flow has often been made because of its simple geometry and fundamental nature to understand the convective heat transfer between fluid and a solid wall. The first attempt on this subject was made by Kim and Moin (1989) for $\mathrm{Pr} = 0.1$, 0.71 and 2.0 with $\mathrm{Re}_\tau = 180$, where Pr is the Prandtl number and Re_τ is the Reynolds number based on the friction velocity

* Corresponding author. E-mail: kawa@muraapl.me.noda.sut.ac.jp.

0142-727X/99/$ – see front matter
PII: S0142-727X(99)00014-4

u_τ and the channel half width δ. Later, Kasagi et al. (1992) and Kasagi and Ohtsubo (1993) made the DNS for $Pr = 0.71$ and 0.025 with a slightly lower Reynolds number of $Re_\tau = 150$. They obtained the budget of the transport equations for the temperature variance, turbulent heat fluxes and their dissipations. Kawamura et al. (1997, 1998) performed the DNS for a wider range of Prandtl numbers from $Pr = 0.025$ up to 5.0 with $Re_\tau = 180$. Recently, Wikström and Johansson (1998) made the DNS with a higher Reynolds number of $Re_\tau = 265$ with a different thermal boundary condition of the uniform temperature difference.

Antonia and Kim (1991) analyzed the DNS data by Kim and Moin (1989) and obtained various turbulence quantities in the near-wall region. Among them, they found that the turbulent Prandtl number Pr_t tends to be a constant level irrespective of the molecular Prandtl number as the wall is approached.

As seen above, most of the DNSs of the turbulent heat transfer in the channel flow have been performed for Reynolds numbers less than $Re_\tau = 180$, which corresponds to $Re_m \simeq 5600$ based on the bulk mean velocity and the channel width. Since this Reynolds number is rather small, the universality of the results should be carefully examined. For example, the logarithmic and the wake regions can hardly be distinguished and the peaks of the turbulent heat fluxes are rather low.

On the other hand, not much work has been done on the DNS of the turbulent channel flow itself with a higher Reynolds number than $Re_\tau = 180$. This is a matter of course because it requires a larger mesh number and longer computational time. Shortly after the well-known DNS with $Re_\tau = 180$ by Kim et al. (1987), the same group performed another with a higher Re_τ of 395 (Kim et al., 1990; Antonia and Kim, 1994). Recently, the present author's group (Kawamura, 1998) performed the DNSs with $Re_\tau = 395$ and 640. In the present work, their DNS of $Re_\tau = 395$ is extended to include the scalar transport with Prandtl numbers of 0.025, 0.20 and 0.71. The results are compared with those of $Re_\tau = 180$ (Kawamura et al., 1997 ; Kawamura et al., 1998) and the effects of the Reynolds and Prandtl numbers are discussed.

2. Fundamental equations and computational method

The flow is assumed to be fully developed and heated by a uniform heat flux q_w from both walls. The computational domain is shown in Fig. 1. The coordinates and flow variables are normalized by the channel half width δ, the friction velocity u_τ, the kinematic viscosity ν and the friction temperature $T_\tau (= q_w/\rho c_p u_\tau)$.

The fundamental non-dimensionalized equations for the velocity field are the continuity equation:

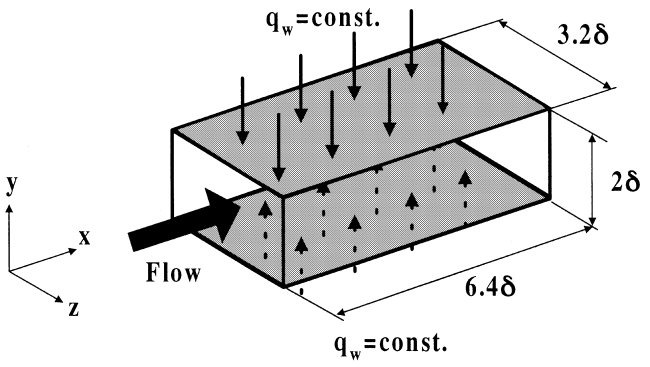

Fig. 1. Computational domain.

$$\frac{\partial u_i^+}{\partial x_i^*} = 0, \tag{1}$$

and the Navier–Stokes equation:

$$\frac{\partial u_i^+}{\partial t^*} + u_j^+ \frac{\partial u_i^+}{\partial x_j^*} = -\frac{\partial p^+}{\partial x_i^*} + \frac{1}{Re_\tau}\frac{\partial^2 u_i^+}{\partial x_j^{*2}}. \tag{2}$$

In this case, the statistically averaged temperature increases linearly with respect to x^*. Then the instantaneous temperature $T^+(x^*, y^*, z^*)$ can be divided into two parts

$$T^+(x^*, y^*, z^*) = \frac{d\langle \overline{T}_m^+ \rangle}{dx^*} x^* - \theta^+(x^*, y^*, z^*), \tag{3}$$

where $\langle \overline{T}_m^+ \rangle$ is the so-called mixed mean temperature defined as

$$\langle \overline{T}_m^+ \rangle = \int_0^1 \overline{u}_1^+ \overline{T}^+ dy^* \Big/ \int_0^1 \overline{u}_1^+ \, dy^*. \tag{4}$$

In the present configuration, its streamwise gradient becomes

$$\frac{d\langle \overline{T}_m^+ \rangle}{dx^*} = 1/\langle \overline{u}^+ \rangle, \tag{5}$$

where $\langle \overline{u}^+ \rangle$ is the velocity averaged over the channel section. With the above transformation, the energy equation becomes

$$\frac{\partial \theta^+}{\partial t^*} + u_j^+ \frac{\partial \theta^+}{\partial x_j^*} = \frac{1}{Re_\tau \cdot Pr}\frac{\partial^2 \theta^+}{\partial x_j^{*2}} + \frac{u_1^+}{\langle \overline{u}^+ \rangle}. \tag{6}$$

The boundary conditions are

$$u_i^+ = 0, \quad \theta^+ = 0 \quad \text{at } y = 0 \text{ and } 2\ \delta. \tag{7}$$

The simulation is made with the use of the finite difference method (see Table 1) in which special attention is paid to the consistency between the analytical and numerical differential operations (Kawamura, 1995). The method was confirmed to give good agreements with the spectral method (Kawamura and Kondoh, 1996). The present numerical scheme consistent with the analytical operation ensures the balance of the transport equations for the statistical correlations such as the turbulent heat flux and the temperature variance. To perform a DNS with a higher Reynolds number, a larger grid number of $256 \times 128 \times 256$ is adopted. The calculation is carried out with the use of a parallel computer, called Numerical Wind Tunnel (NWT) located at National Aerospace Laboratory.

The computational and visualized conditions are given in Table 1.

Table 1
Computational and visualized conditions

Grid	Staggered grid
Coupling algorithm	Fractional step method
Time advancement	
Viscous term (y-direction)	2nd-order Crank–Nicolson Method
Others	2nd-order Adams–Bashforth Method
Discretization scheme	
Nonlinear terms	2nd-order central scheme (Consistent)
Viscous terms	2nd-order central scheme
Boundary condition	Periodic(x, z direction), Non-slip (y-direction)
Grid number	$128 \times 66 \times 128$ ($Re_\tau = 180$), $256 \times 128 \times 256$ (395)
Computational volume	$6.4\delta \times 2\delta \times 3.2\delta$
Visualized volume	$3.2\delta \times \delta \times 1.6\delta$
Reynolds number	$Re_\tau = 180$, 395
Prandtl number	$Pr = 0.025$, 0.2, 0.71

3. Results

3.1. Velocity field

To examine the obtained velocity field, the mean velocity profile and the rms of the Reynolds normal stress are shown and compared with those by Kim et al. (1990) in Figs. 2 and 3. Although a small discrepancy is observed, the agreement is good enough.

3.2. Mean temperature profile

The mean temperature is given for two Reynolds numbers of 180 and 395 and for Prandtl numbers of 0.025, 0.20 and 0.71 in Fig. 4. The one by Kasagi's group ($Pr = 0.025$ and 0.71 for $Re_\tau = 150$) is also plotted for comparison. Similar to the mean velocity distribution, there exists the logarithmic region in the mean temperature profile, too:

$$\overline{\theta}^+ = \frac{1}{\kappa_\theta} \ln y^+ + c_\theta, \tag{8}$$

where κ_θ is the von Karman constant of the mean temperature profile. In the present calculation, the logarithmic region can be better distinguished from the wake region with the increase of the Reynolds and Prandtl numbers.

With the use of the present DNS data, κ_θ can be obtained by

$$\frac{1}{\kappa_\theta} = y^+ \frac{d\overline{\theta}^+}{dy^+}. \tag{9}$$

The resultant κ_θ is shown in Fig. 5. In case of $Re_\tau = 180$, no plateau is observed for $Pr = 0.2$; while for $Pr = 0.71$, κ_θ exhibits a plateau. In case of $Re_\tau = 395$, the plateau can be seen for both $Pr = 0.2$ and 0.71. Moreover, κ_θ decreases significantly after the plateau ends, which corresponds to the distinction between the logarithmic and wake regions. It is interesting to note that, in case of $Re_\tau = 395$, the values of κ_θ for $Pr = 0.71$ and 0.2 become roughly independent of the Prandtl number for $y^+ > 50$. This means that the semi-logarithmic plots of the mean temperature become parallel for $Pr \geqslant 0.2$, which can be confirmed in Fig. 4.

Kader (1981) proposed $\kappa_\theta = 0.47$ independently of Pr in his empirical correlation. The present DNS supports the independence; however, the value of the κ_θ itself is somewhat smaller than his proposal and is closer to the von Karman constant of the mean velocity profile ($\kappa_u \simeq 0.4 \sim 0.42$).

3.3. Temperature variance

The rms of the temperature variance is shown in Fig. 6 for various Reynolds and Prandtl numbers. When the Prandtl number is large enough, e.g., $Pr = 0.71$, the peak value depends only weakly upon the Reynolds number. For a smaller Prandtl number, however, the peak increases as the Reynolds number does.

The ratio θ'^+_{rms}/Pr is plotted logarithmically in Fig. 7 to emphasize the near-wall behavior. In the wall vicinity, the

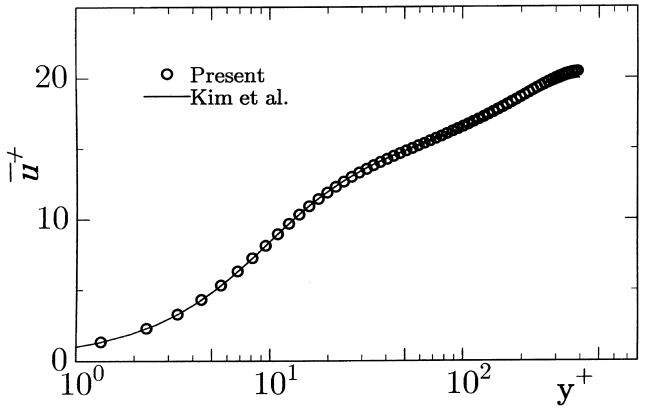

Fig. 2. Mean velocity profile ($Re_\tau = 395$) in comparison with Kim et al. (1990).

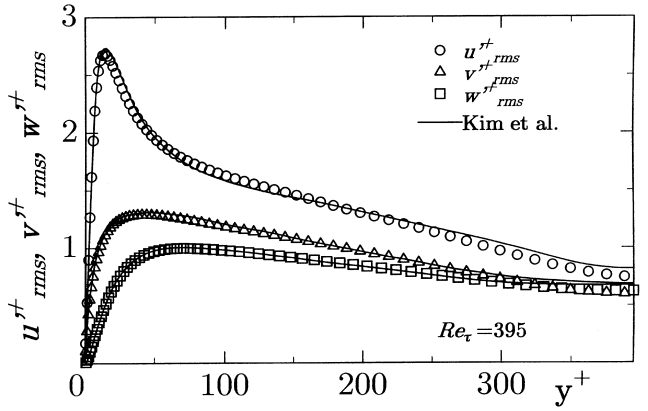

Fig. 3. Rms of Reynolds normal stress ($Re_\tau = 395$) in comparison with Kim et al. (1990).

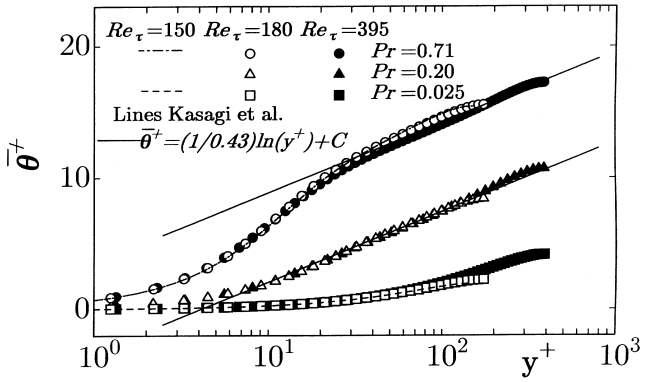

Fig. 4. Mean temperature profiles.

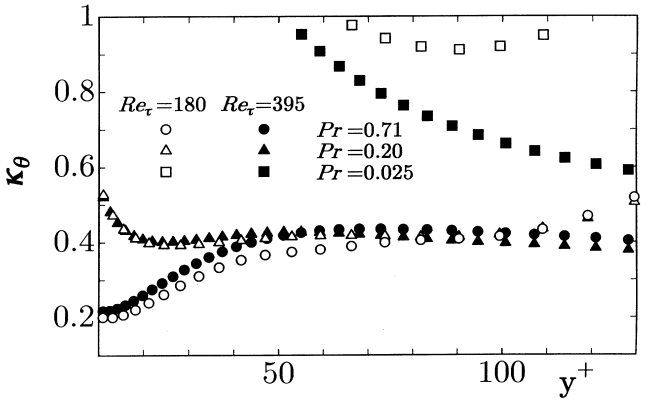

Fig. 5. κ_θ of mean temperature.

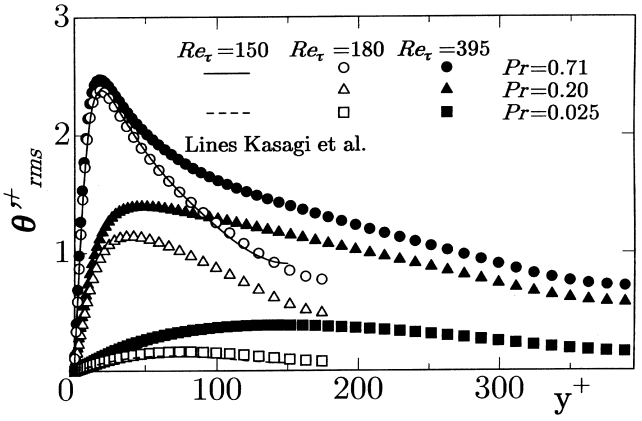

Fig. 6. Rms of temperature variance.

fluctuation of the temperature is expanded usually (Antonia and Kim, 1991) in terms of y^+ as

$$\theta'^{+} = \tilde{b}_\theta y^{+} + \tilde{c}_\theta y^{+^2} + \cdots. \tag{10}$$

In the previous paper (Kawamura et al., 1998), the author's group proposed a new expansion of

$$\theta'^{+} = \mathrm{Pr}(b_\theta y^{+} + c_\theta y^{+^2} + \cdots). \tag{11}$$

For this expansion to be valid, the expansion coefficient b_θ must be independent of Pr. To examine this point, the ratio $\theta'^{+}_{\mathrm{rms}}/Pry^{+}$ is plotted in Fig. 8. In case of $\mathrm{Re}_\tau = 180$, b_θ is still dependent on Pr in the whole range of the present calculation. In case of $\mathrm{Re}_\tau = 395$, however, b_θ becomes independent of Pr for $\mathrm{Pr} \geqslant 0.2$. Thus, the expansion of Eq. (11) can be confirmed to be valid if the Reynolds and Prandtl numbers are higher than a certain limit.

3.4. Wall-normal turbulent heat flux

The wall-normal turbulent heat flux is plotted in Fig. 9 with emphasis on the near-wall region. Considering the expansion of Eq. (11) and a similar one for v'^{+}:

$$v'^{+} = c_2 y^{+2} + \cdots, \tag{12}$$

the wall-normal turbulent heat flux can be expressed in terms of y^+ as

$$-\overline{v' + \theta'^{+}} = -\mathrm{Pr}\ \overline{b_\theta c_2} y^{+^3} + \cdots. \tag{13}$$

Fig. 9 indicates that the dependence of the correlation coefficient $\overline{b_\theta c_2}$ upon the Reynolds number is not large but still appreciable; i.e. $\overline{b_\theta c_2} \simeq 0.0008$ for $\mathrm{Re}_\tau = 180$ and 0.001 for 395.

Since a fully developed flow is assumed, the sum of the wall-normal turbulent and the molecular heat fluxes satisfies the following relation.

$$\frac{1}{\mathrm{Pr}}\frac{\mathrm{d}\overline{\theta}^{+}}{\mathrm{d}y^{+}} - \overline{v'^{+}\theta'^{+}} = 1 - \frac{\int_0^{y^+} \overline{u}_1^{+}\,\mathrm{d}y^{+}}{\langle \overline{u}^{+} \rangle \mathrm{Re}_\tau}, \tag{14}$$

which is equal to the total heat flux q^+_{total}. The total and the wall-normal turbulent heat fluxes are shown in Fig. 10. The peak of the turbulent heat flux increases with the increase of the Re_τ and Pr. The peak arises at around $y^+ = 30$–60 for $\mathrm{Pr} \geqslant 0.2$, while $y^+ > 50$ for $\mathrm{Pr} = 0.025$.

The peak value of the wall-normal turbulent flux can be estimated as follows. Firstly, the total heat flux is expressed as

$$q^+_{\mathrm{total}} = \frac{1}{\mathrm{Pr}}\frac{\mathrm{d}\overline{\theta}^{+}}{\mathrm{d}y^{+}} - \overline{v'^{+}\theta'^{+}} = 1 - \frac{y^{+}}{\mathrm{Re}_\tau} + \phi(y^{+}), \tag{15}$$

where $\phi(y^+)$ is a small correction function depending on the velocity profile. It can be empirically approximated as

$$\phi(y^{+}) = b\frac{y^{+}}{\mathrm{Re}_\tau}\left(1 - \frac{y^{+}}{\mathrm{Re}_\tau}\right)^2, \tag{16}$$

where b is an empirical constant of about 0.4. If the logarithmic profile is assumed for the mean temperature, then its gradient becomes

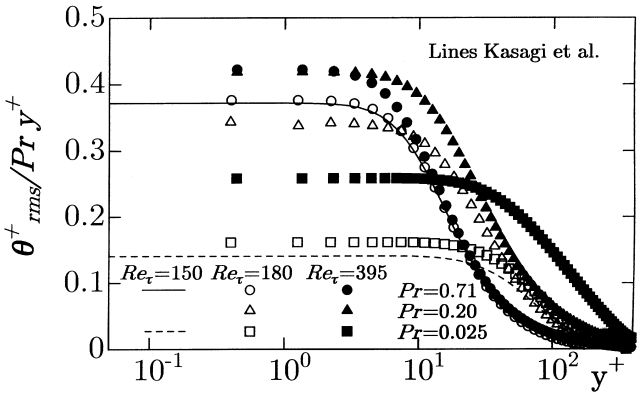

Fig. 8. Ratio of $\theta'^{+}_{\mathrm{rms}}/\mathrm{Pr}y^{+}$.

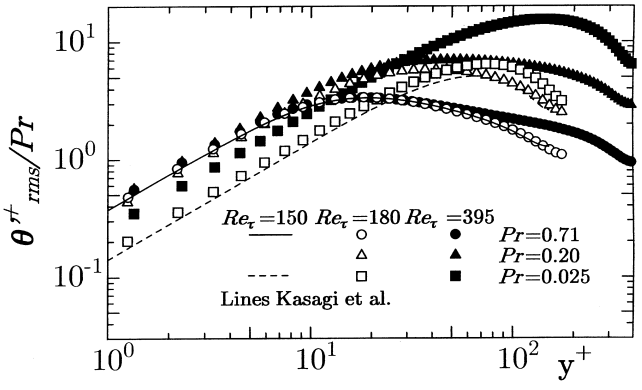

Fig. 7. Ratio of $\theta'^{+}_{\mathrm{rms}}/\mathrm{Pr}$.

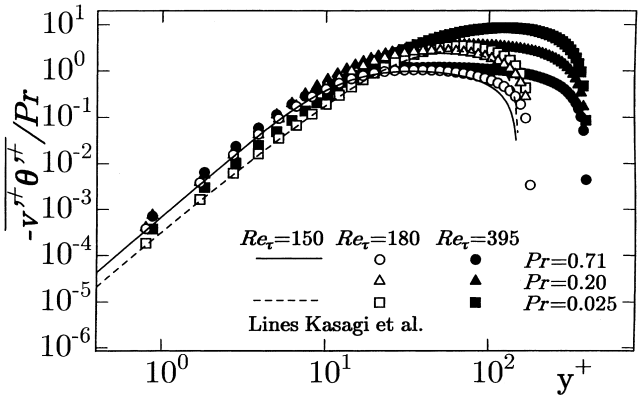

Fig. 9. Logarithmic plot of wall-normal turbulent heat flux.

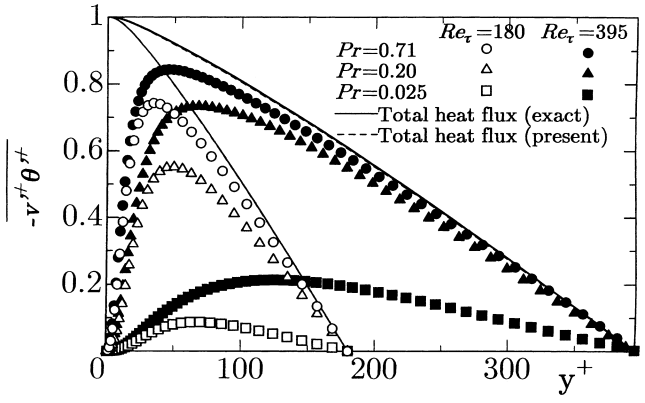

Fig. 10. Total and turbulent heat fluxes.

$$\frac{d\overline{\theta}^+}{dy^+} = \frac{1}{\kappa_\theta y^+}. \tag{17}$$

With the use of Eqs. (16) and (17), Eq. (15) gives

$$-\overline{v'^+\theta'^+} = 1 - \frac{1}{\kappa_\theta \mathrm{Pr} y^+} - (1-b)\frac{y^+}{\mathrm{Re}_\tau} - 2b\left(\frac{y^+}{\mathrm{Re}_\tau}\right)^2 + b\left(\frac{y^+}{\mathrm{Re}_\tau}\right)^3. \tag{18}$$

If the last two higher order terms are neglected for simplicity, the peak of $-\overline{v'^+\theta'^+}$ arises at

$$y^+_{\max} = \sqrt{\frac{1}{(1-b)}\frac{\mathrm{Re}_\tau}{\kappa_\theta \mathrm{Pr}}}. \tag{19}$$

Then the peak value becomes

$$-\overline{v'^+\theta'^+}_{\max} \simeq 1 - 2\sqrt{\frac{1-b}{\kappa_\theta \mathrm{Pe}_\tau}} - \frac{2b}{1-b}\frac{1}{\kappa_\theta \mathrm{Pe}_\tau} + \frac{b}{(1-b)^{3/2}} \times \frac{1}{(\kappa_\theta \mathrm{Pe}_\tau)^{3/2}}, \tag{20}$$

where $\mathrm{Pe}_\tau = \mathrm{Pr} \cdot \mathrm{Re}_\tau$ is the Peclet number. This correlation is compared with the DNS results in Fig. 11, where good agreement is obtained.

The cross-correlation coefficient of the wall-normal turbulent heat flux is shown in Fig. 12, in which that of the Reynolds shear stress R_{uv} is also plotted. The cross-correlation coefficient $R_{v\theta}$ decreases with the increase of the Prandtl number for a given Reynolds number. When the Prandtl number becomes closer to unity, $R_{v\theta}$ coincides well with R_{uv} for both Reynolds numbers. This indicates that the smaller $R_{v\theta}$ compared with $R_{u\theta}$ is caused by the lower correlation between u'^+ and v'^+. For a higher Reynolds number, the dependence of $R_{v\theta}$ upon Pr decreases, because the convective effect is more enhanced.

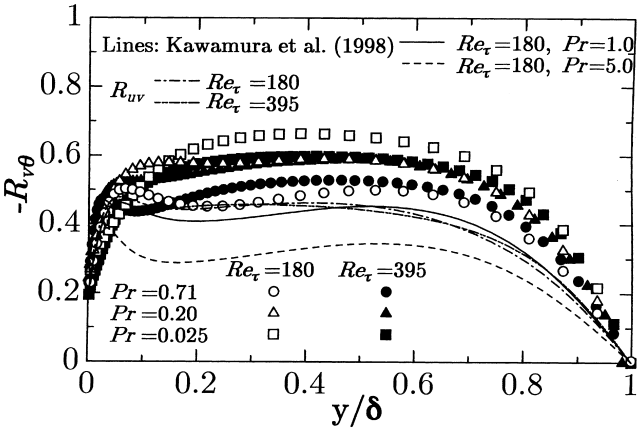

Fig. 12. Cross-correlation coefficient of wall-normal turbulent heat flux.

3.5. Streamwise turbulent heat flux

The streamwise turbulent heat flux is given in Fig. 13. Its peak is determined primarily by the Prandtl number and it increases with the increase of Pr. The dependence of the peak value on the Reynolds number is already negligible for $\mathrm{Pr} = 0.71$ but is still appreciable for $\mathrm{Pr} = 0.2$ and 0.025. It is interesting to note that, in the central region of the channel, the streamwise heat flux does not depend on the Prandtl number if $\mathrm{Pr} \geqslant 0.2$.

The cross-correlation coefficient of the streamwise turbulent heat flux is shown in Fig. 14. When the Prandtl number is smaller than 1.0, the cross-correlation coefficient $R_{u\theta}$ increases with the increase of the Prandtl number for both Reynolds numbers. On the other hand, when the Prandtl number is larger than 1.0, $R_{u\theta}$ decreases with the increase of Pr because the similarity of the velocity and thermal fields is lost. In case of $\mathrm{Re}_\tau = 180$, the maximum value of $R_{u\theta}$ reaches even 0.97 at $y^+ \simeq 7$ with $\mathrm{Pr} = 1.0$. For $\mathrm{Re}_\tau = 395$, that of $R_{u\theta}$ is 0.94 at $y^+ \simeq 8$ with $\mathrm{Pr} = 0.71$. These high values of $R_{u\theta}$ result from the quasi-coherent structures, e.g., streaks. Moreover, the fluctuating

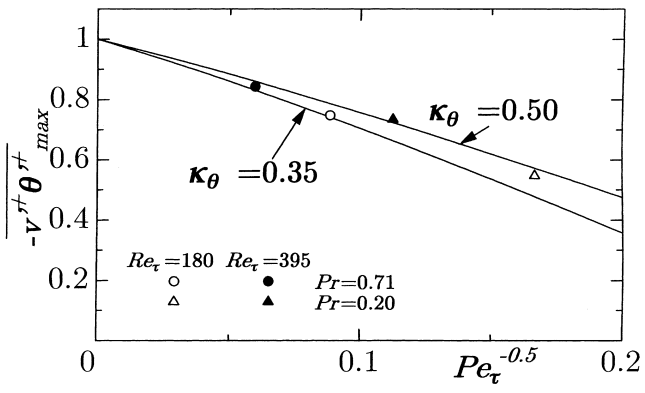

Fig. 11. Peak value of wall-normal turbulent heat flux.

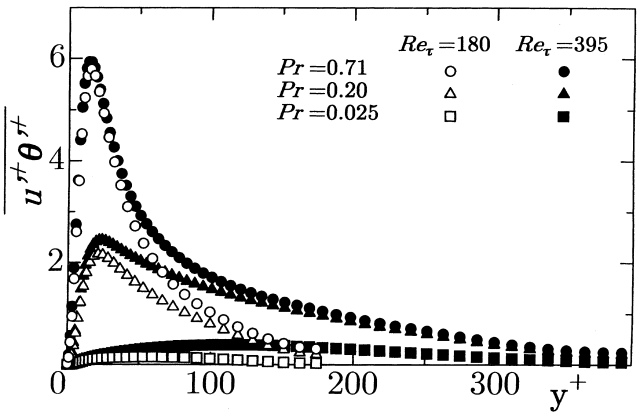

Fig. 13. Streamwise turbulent heat flux.

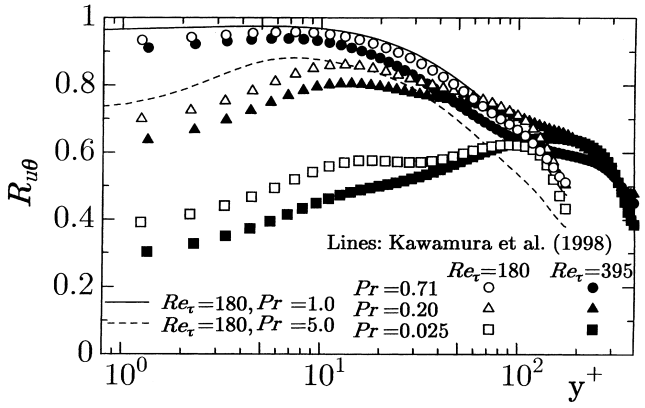

Fig. 14. Cross-correlation coefficient of streamwise turbulent heat flux.

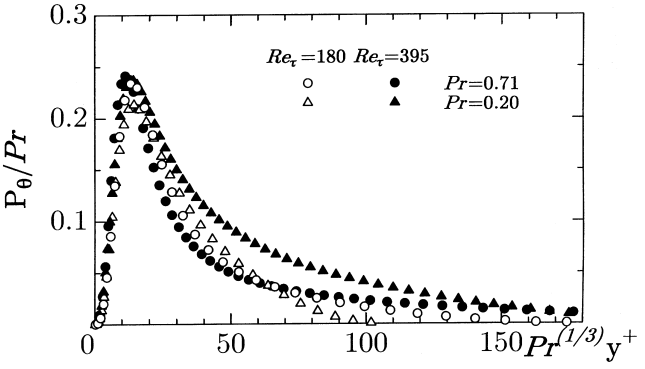

Fig. 16. Production term P_θ for temperature variance.

streamwise velocity (u'^+) is much larger than the wall-normal one (v'^+), because the latter is bound by the wall but the former is not. These are the reasons why the streamwise turbulent heat flux is much larger than the wall-normal one.

3.6. Budgets of transport equations

The budgets of the transport equation for the temperature variance are compared for $Re_\tau = 180$ and 395 in Fig. 15. The budget terms are non-dimensionalized by the factor of $u_\tau^3 T_\tau/\nu$. Both the production and dissipation terms increase with the increase of the Reynolds number. The present authors (Kawamura et al., 1997 ; Kawamura et al., 1998) examined a scaling law of the peak of the production term P_θ for the temperature variance and found that it can be scaled by P_θ/Pr and $Pr^{1/3}y^+$. As shown in Fig. 16, this scaling law is better satisfied with the increase of the Reynolds number.

The budgets for the wall-normal turbulent heat flux are shown in Figs. 17–20. These indicate that the dominating terms increase with the increase of Reynolds number. The Reynolds number effect seems to be more pronounced for a smaller Prandtl number of 0.025. When the Prandtl number is 0.71, the production and temperature pressure-gradient correlation (TPG) terms are dominant and the dissipation term is considerably small; while, at $Pr = 0.025$, the production and dissipation terms are prominent and TPG term is negligible. This point was already well recognized and taken into account in the modeling of the turbulent heat transport (Launder, 1976). In case of $Pr = 0.2$, however, both the TPG and the dissipation terms contribute comparatively (see Fig. 19).

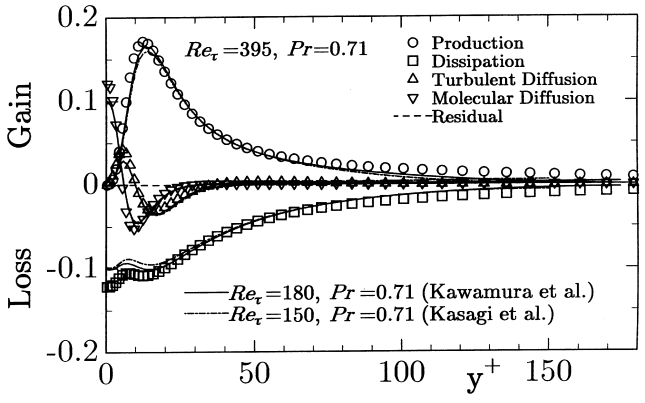

Fig. 15. Budget of temperature variance ($Re_\tau = 395, Pr = 0.71$).

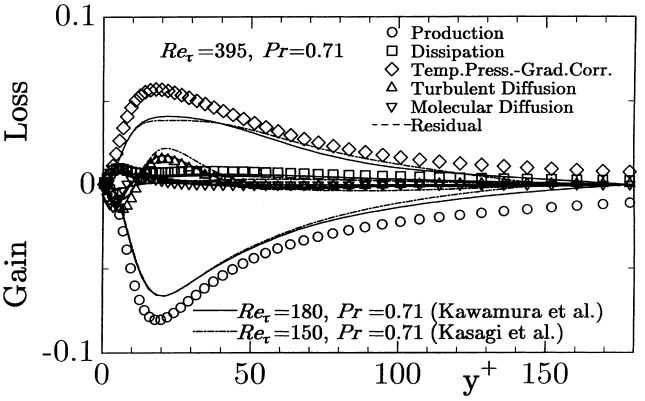

Fig. 17. Budget of wall-normal turbulent heat flux ($Re_\tau = 395$, $Pr = 0.71$).

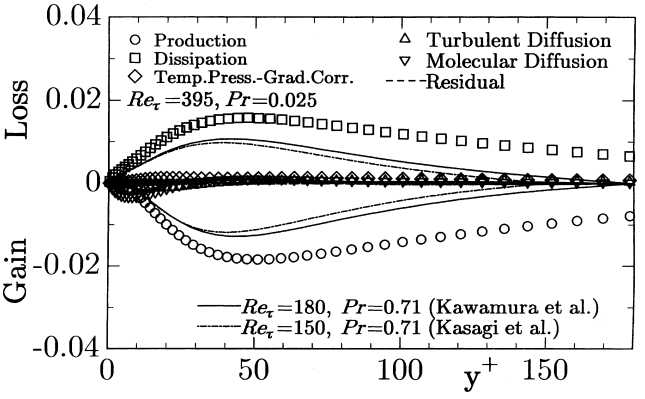

Fig. 18. Budget of wall-normal turbulent heat flux ($Re_\tau = 395$, $Pr = 0.025$).

Comparison of Fig. 19 and Fig. 20 indicates that, with the increase of the Reynolds number, the dissipation term stays rather unchanged while the TPG term increases to contribute more dominantly to the budget.

3.7. Turbulent Prandtl number and time scale ratio

The turbulent Prandtl number is an important quantity in the engineering heat transfer calculation. It is defined as

$$\mathrm{Pr_t} = \frac{\nu_t}{a_t} = \frac{\overline{u'^+v'^+}}{\overline{v'^+\theta'^+}} \frac{(\mathrm{d}\overline{\theta}^+/\mathrm{d}y^+)}{(\mathrm{d}\overline{u_1}^+/\mathrm{d}y^+)}. \tag{21}$$

There has been a long discussion on the dependence of the Prandtl number upon the wall-normal distance y^+ and/or the molecular Prandtl number. Antonia and Kim (1991) found that the turbulent Prandtl number becomes almost independent of both y^+ and Pr as the wall is approached except for a very low Prandtl number. In addition to the near-wall expansion of θ'^+ and v'^+ in Eqs. (11) and (12), the mean temperature and the velocity fields can be expanded as follows:

$$\overline{\theta}^+ = \mathrm{Pr}y^+ + \cdots, \tag{22}$$

$$\overline{u}^+ = y^+ + \cdots, \tag{23}$$

$$u'^+ = b_1 y^+ + c_1 y^{+2} + \cdots \quad (y^+ \to 0). \tag{24}$$

Accordingly, the Reynolds shear stress can be obtained as

$$\overline{u'^+v'^+} = \overline{b_1 c_2} y^{+3} + \cdots. \tag{25}$$

With the use of Eqs. (13), (22), (23) and (25), the turbulent Prandtl number becomes

$$\mathrm{Pr}_t = \frac{\overline{b_1 c_2} y^{+3} \mathrm{Pr}}{\mathrm{Pr}\overline{c_2 b_\theta} y^{+3}} = \frac{\overline{b_1 c_2}}{\overline{c_2 b_\theta}}. \tag{26}$$

The correlation coefficient $\overline{b_\theta c_2}$ may still depend upon Pr. However the main part of the dependence upon Pr is already extracted from $\overline{b_\theta c_2}$ by the form of Eq. (13), the effect of Pr upon $\overline{b_\theta c_2}$ can be expected to be small. The other coefficient of $\overline{b_1 c_2}$ is independent of Pr. It depends upon the Reynolds number only, but its dependency is rather small. Thus, one can expect that the turbulent Prandtl number becomes almost independent of Reynolds and Prandtl numbers as the wall is approached.

The turbulent Prandtl number is plotted in Fig. 21 including the present DNS of $\mathrm{Re}_\tau = 395$. The wall asymptotic value of $\mathrm{Pr_t}$ for $\mathrm{Pr} \geqslant 0.2$ is certainly independent of y^+ and Prandtl number irrespective of the Reynolds number.

On the other hand, $\mathrm{Pr_t}$ of the lower Prandtl number ($\mathrm{Pr} = 0.025$) depends significantly upon the Reynolds number. It moves towards the normal value for the larger Pr. Thus it is indicated that the very high value of $\mathrm{Pr_t}$ for a low Prandtl number fluid is caused by the effect of the low Reynolds number. With the increase of the Reynolds number, the convection transport contributes more dominantly compared to the conduction effect.

The time scale ratio defined as

$$R = \frac{\overline{\theta'^{+2}}\varepsilon}{2k\varepsilon_\theta} \tag{27}$$

is a quantity often used to estimate the dissipation rate of the temperature variance. Its wall asymptotic value is exactly equal to the molecular Prandtl number. Fig. 22 shows the distribution of the time scale ratio for the Reynolds and Prandtl numbers calculated. Its wall value is indeed equal to Pr. The dependence upon the Reynolds number seems not so large for all the Prandtl numbers calculated.

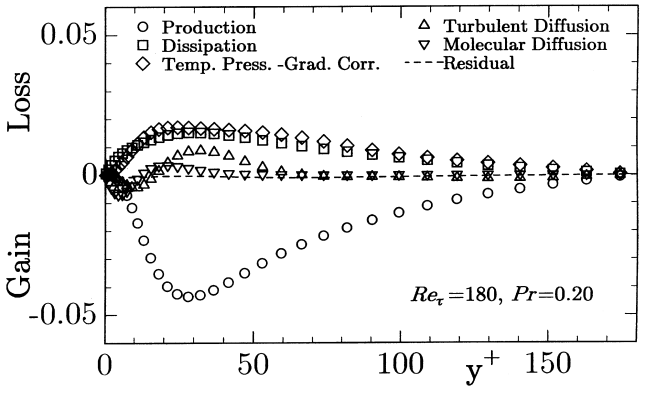

Fig. 19. Budget of wall-normal turbulent heat flux ($\mathrm{Re}_\tau = 180$, $\mathrm{Pr} = 0.20$).

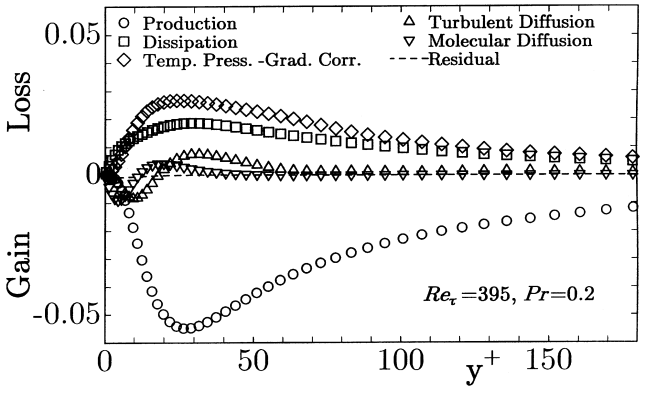

Fig. 20. Budget of wall-normal turbulent heat flux ($\mathrm{Re}_\tau = 395$, $\mathrm{Pr} = 0.20$).

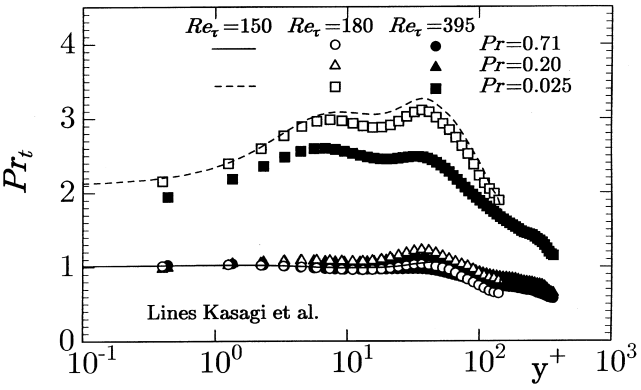

Fig. 21. Distribution of turbulent Prandtl number.

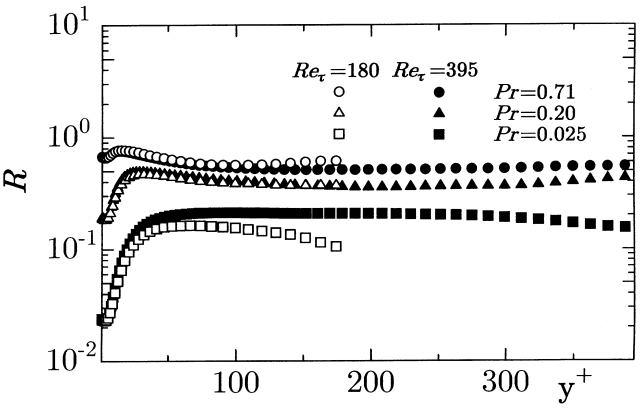

Fig. 22. Distribution of time scale ratio.

Fig. 23. (a) High- and low-speed streaks and low-pressure regions ($Re_\tau = 180$) ($u'^+ > 3.0$: dark-gray, $u'^+ < -3.0$: light-gray, $p'^+ < -3.0$: white). (b) High- and low-speed streaks and low-pressure regions ($Re_\tau = 395$) ($u'^+ > 3.0$: dark-gray, $u'^+ < -3.0$: light-gray, $p'^+ < -3.0$: white).

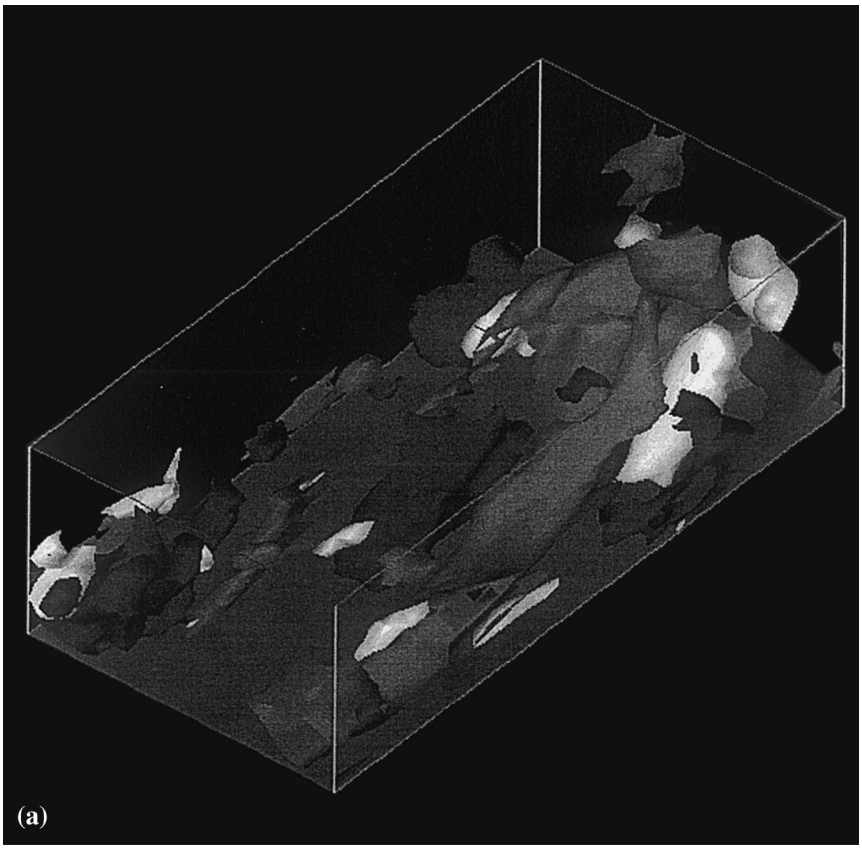

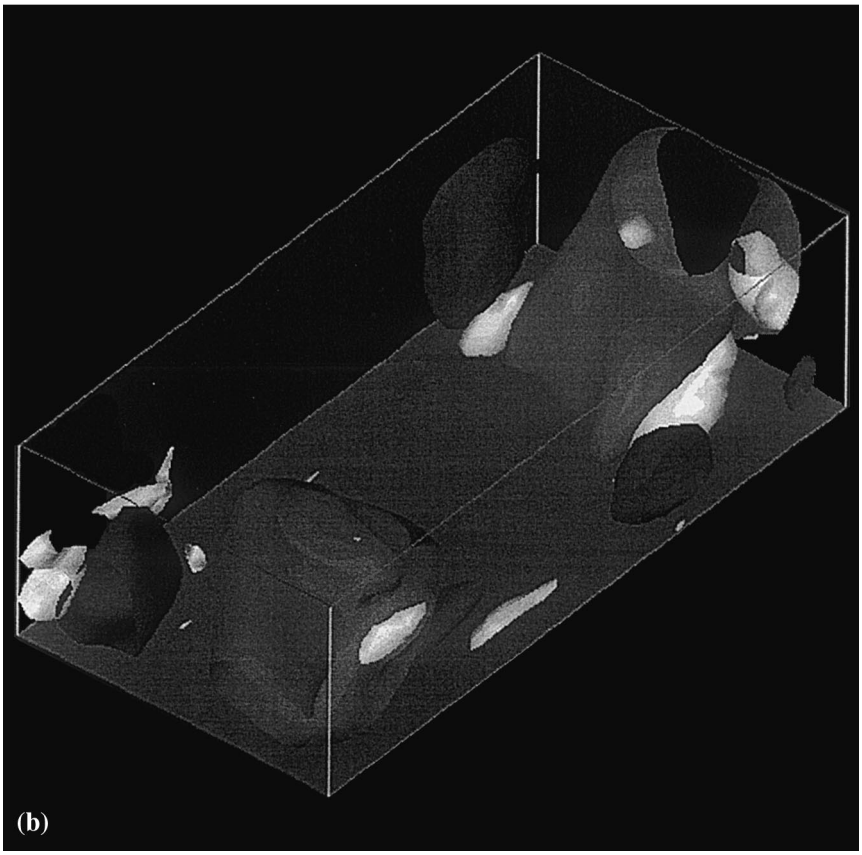

Fig. 24. (a) High- and low-temperature regions and low-pressure regions ($\mathrm{Re}_\tau = 180, \mathrm{Pr} = 0.71$) ($T'^+ > 3.0$: light-gray, $T'^+ < -3.0$: dark-gray, $p'^+ < -3.0$: white). (b) High- and low-temperature regions and low-pressure regions ($\mathrm{Re}_\tau = 180, \mathrm{Pr} = 0.025$) ($T'^+ > 0.22$: light-gray, $T'^+ < -0.22$: dark-gray, $p'^+ < -3.0$: white).

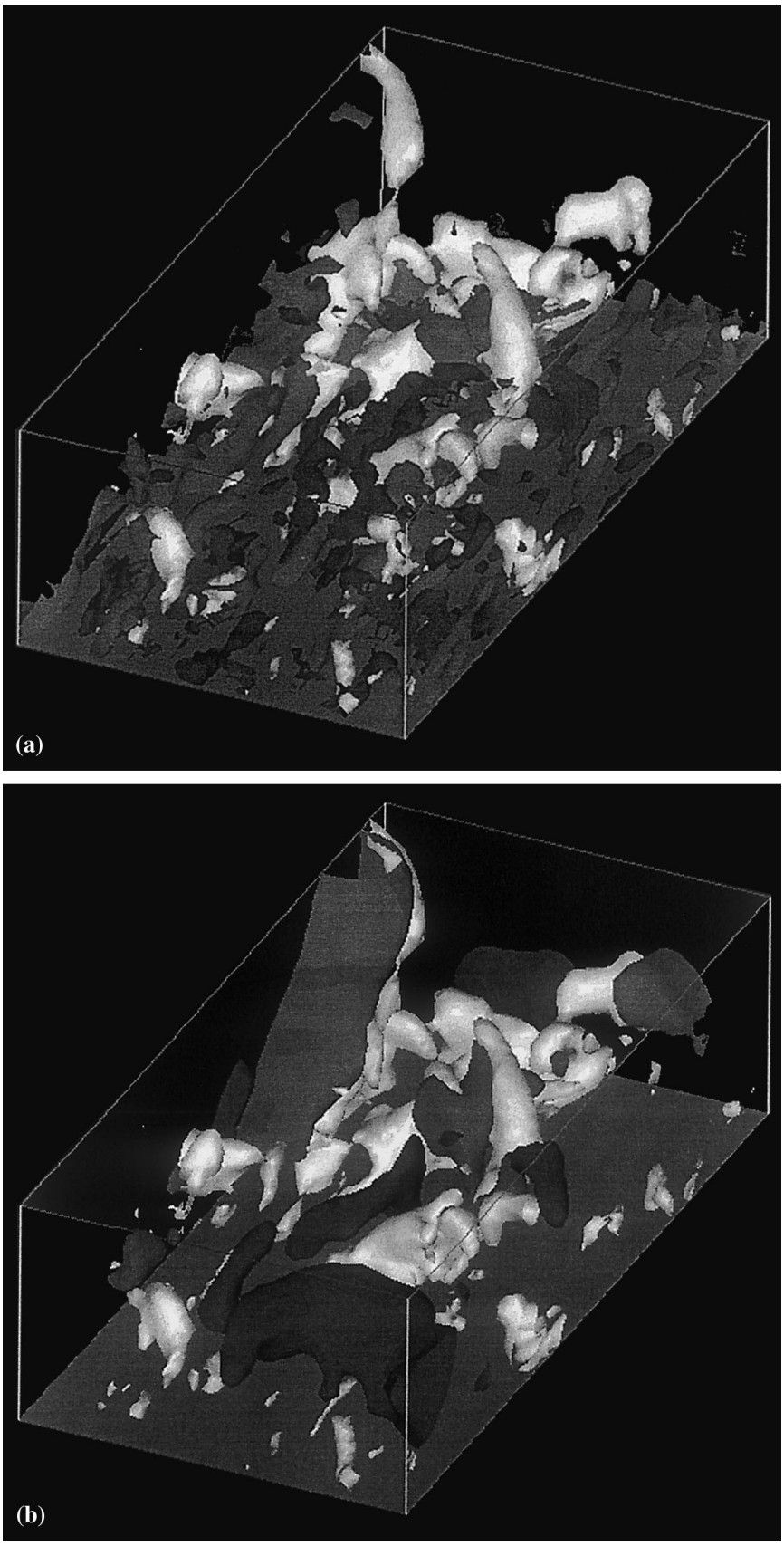

Fig. 25. (a) High- and low-temperature regions and low-pressure regions ($\mathrm{Re}_\tau = 395, \mathrm{Pr} = 0.71$) ($T'^+ > 3.0$: light-gray, $T'^+ < -3.0$: dark-gray, $p'^+ < -3.0$: white). (b) High- and low-temperature regions and low-pressure regions ($\mathrm{Re}_\tau = 395, \mathrm{Pr} = 0.025$) ($T'^+ > 0.40$: light-gray, $T'^+ < -0.40$: dark-gray, $p'^+ < -3.0$: white).

3.8. Instantaneous velocity and temperature fields

The instantaneous velocity and thermal fields are visualized to investigate the streaky and vortical structures with the use of DNS data in Figs. 23–25. The visualized volume is one eighth of the computational domain ($3.2\delta \times \delta \times 1.6\delta$), which corresponds to $576 \times 180 \times 288$ in terms of the wall unit (ν/u_τ) for $Re_\tau = 180$ and $1264 \times 395 \times 632$ for $Re_\tau = 395$. Note that the fluid flows from the bottom left to the top right and that the sign of the temperature fluctuation is inversed ($T'^+ = -\theta'^+$) to meet an intuitive impression of the heating wall.

Instantaneous velocity fields are compared for $Re_\tau = 180$ and 395 in Fig. 23(a) and (b), where the contour surfaces of high- and low-speed streaks and the low-pressure region are visualized. The high- and low-speed streaks imply $+u'^+$ and $-u'^+$, where u'^+ represents the fluctuating part of the streamwise velocity.

It is well known that the low-pressure region corresponds to the core of vortical structures as discussed by Robinson (1991). When the Reynolds number increases, the structures become highly intermittent in space. In case of a low Reynolds number, only limited types of vortical structures are observed. On the other hand, with the increase of the Reynolds number, various shapes of the vortices appear. The well-known hairpin vortex is not observed, but many single vortices are dominant. Some of them look like the so-called banana vortices (Robinson, 1991).

The elongated streaky structure is obtained for both Re_τs. The low-speed streaks are longer than the high-speed ones as reported by Robinson (1991). The spanwise spacing of the low-speed streaks is approximately 100 in the wall units, which is in accordance with the experimental knowledge. In addition, the low-speed streaks are generally elongated more than 1000 wall units in the streamwise direction.

The temperature field is visualized and shown for $Pr = 0.71$ and 0.025 with $Re_\tau = 180$ and 395 in Fig. 24(a) and (b) and Fig. 25(a) and (b), where the contour surfaces of high- and low-temperature regions and the low-pressure region are visualized. The high- and low-temperature regions imply $+T'^+$ and $-T'^+$, where T'^+ represents the fluctuating part of the temperature. Note that figures (a) and (b) in Figs. 24 and 25 illustrate the temperature contour based on the same velocity field.

In case of $Pr = 0.71$, the velocity and the thermal streaky structures show a strong resemblance with each other for both of the Reynolds numbers. In case of a low Prandtl number of $Pr = 0.025$, the thermal streaks are not so elongated in the streamwise direction and their spanwise spacing seems to be larger (Kasagi and Ohtsubo, 1993) compared with that of $Pr = 0.71$ for both Re_τ's. Moreover, the high- and low-temperature regions exist away from the wall in accordance with the peak position of the temperature fluctuations independent of the Reynolds number. When the Reynolds number is large as $Re_\tau = 395$, however, the streaks are more elongated than those of $Re_\tau = 180$, because the convective effect becomes more enhanced than the conductive one with the increase of the Reynolds number.

4. Concluding remarks

The DNS of turbulent channel flow with scalar transport was performed for the Reynolds numbers of $Re_\tau = 180$ and 395. The molecular Prandtl numbers were 0.025, 0.2 and 0.71. Turbulence statistics such as the temperature variance, the turbulent heat fluxes, their budget terms, the turbulent Prandtl number and the time scale ratio were obtained and the effects of the Reynolds and Prandtl numbers were discussed. The conclusions derived are as follows:

1. In the mean temperature profile, the logarithmic and wake regions were better distinguished with the increase of Re_τ.
2. The temperature variance and the streamwise and wall-normal heat fluxes were obtained and their expansion coefficient in the wall vicinity was examined.
3. The near-wall value of the turbulent Prandtl number (Pr_t) was found to be about unity independent of both Re_τ and Pr if $Pr \geqslant 0.2$. The effect of the Reynolds number on Pr_t was more significant for a lower molecular Prandtl number.
4. Instantaneous flow and temperature fields were visualized and their structures were compared for two different Reynolds numbers.

The present database will be open to public access. Detailed information is given at http://muraibm.me.noda.sut.ac.jp/e-page1.html.

Acknowledgements

This simulation was performed with the use of the Numerical Wind Tunnel (NWT) of National Aerospace Laboratory. The authors are grateful to Dr. K. Yamamoto of NAL for his helpful supports in the preparation and execution of the computation on NWT.

References

Antonia, R.A., Kim, J., 1991. Turbulent Prandtl number in the near-wall region of a turbulent channel flow. Int. J. Heat Mass Trans. 34, 1905–1908.

Antonia, R.A., Kim, J., 1994. Low-Reynolds-number effects on near-wall turbulence. J. Fluid Mech. 276, 61–80.

Kader, B.A., 1981. Temperature and concentration profiles in fully turbulent boundary layers. Int. J. Heat Mass Trans. 24, 1541–1544.

Kasagi, N., Tomita, Y., Kuroda, A., 1992. Direct numerical simulation of passive scalar field in a turbulent channel flow. ASME J. Heat Trans. 114, 598–606.

Kasagi, N., Ohtsubo, Y., 1993. Direct numerical simulation of low Prandtl number thermal field in a turbulent channel flow. In: Durst, F. et al. (Eds.), Turbulent Shear Flows, vol. 8, Springer, Berlin, pp. 97–119.

Kawamura, H., 1995. Direct numerical simulation of turbulence by finite difference scheme. In: The Recent Developments in Turbulence Research. International Academic Publishers, pp. 54–60.

Kawamura, H., Kondoh, Y., 1996. Application of consistent finite difference scheme to DNS of turbulent heat transfer in channel flow. In: Proceedings of the Third KSME-ASME Thermal Engineering Conference, vol. 1, Kyongju, pp. 53–58.

Kawamura, H., Ohsaka, K., Yamamoto, K., 1997. DNS of turbulent heat transfer in channel flow with low to medium-high Prandtl number fluid. In: Proceedings of the 11th Symposium Turbulent Shear Flows, vol. 1, Grenoble, pp. 8.7–8.12.

Kawamura, H., Ohsaka, K., Abe, H., Yamamoto, K., 1998. DNS of turbulent heat transfer in channel flow with low to medium-high Prandtl number. Int. J. Heat and Fluid Flow 19, 482–491.

Kawamura, H., 1998. Direct numerical simulation of turbulence by parallel computation. Proceedings of the 10th Parallel CFD Conference, Hsinchu, Taiwan, in press.

Kim, J., Moin, P., Moser, R., 1987. Turbulence statistics in fully developed turbulent channel flow at low Reynolds number. J. Fluid Mech. 177, 133–166.

Kim, J., Moin, P., Moser, R., 1990. In: Bradshaw, P. (Ed.), The diskette of Collaborative testing of turbulence models. Stanford University.

Kim, J., Moin, P., 1989. Transport of passive scalars in a turbulent channel flow. In: Andre, J.-C. et al. (Eds.), Turbulent Shear Flows, vol. 6, Springer, Berlin, pp. 85–96.

Launder, B.E., 1976. Heat and mass transport. In: Bradshow, P. (Ed.), Turbulence, Topics in Applied Physics. Springer, Berlin, pp. 231–287.

Robinson, S.K., 1991. The kinematics of turbulent boundary layer structure. NASA TM-103859.

Wikström, P.M., Johansson, A.V., 1998. DNS and scalar-flux transport modeling in a turbulent channel flow. Proceedings of the 2nd EF Conference in Turbulent Heat Transfer, vol. 1, Manchester, UK, pp. 6.46–6.51.